Comparison of Local Kernel and Covariance Matrix Descriptors for Spatial-Spectral Classification of Hyperspectral Images

Behnam Asghari Beirami*, Mehdi Mokhtarzade

Department of Photogrammetry and Remote Sensing, K. N. Toosi University of Technology, Tehran, Iran, m_mokhtarzade@kntu.ac.ir
* Corresponding author; behnam.asghari1370@gmail.com

Abstract

Hyperspectral sensors collect information from the earth's surface in the form of images with a large number of electromagnetic bands. Accurate classification of hyperspectral images has been one of the hot topics in remote sensing. Spatial information as a complementary source for spectral information helps increase the classification accuracy of hyperspectral images (HSI). Local covariance matrix descriptor (LCMD) is the new spatial-spectral feature generation method for HSI classification. Although the LCMD is easy to use and performs well in HSI classification, it has some limitations, such as discarding the nonlinear relationships between features, which are useful in HSI classification. To address these issues, we propose a local kernel matrix descriptor (LKMD) for the classification of HSIs. In this study, the performance of LCMD is compared with LKMD with two widely used kernels, RBF and polynomial, and final classification results on two real HSIs, Indian Pines and Pavia University, proved the superiority of LKMD over LCMD.

Keywords: Electric vehicles, Day-ahead scheduling, Optimal charging, Power markets, Copula
Article history: Submitted 05-Mar-2022; Revised 02-May-2022; Accepted 04-May-2022. Article Type: Research paper

https://doi.org/10.30495/ijsee.2022.1954291.1179

1. Introduction

Hyperspectral imagery (HSI), which contains a wide range of spectral bands, can be applied to study various surface phenomena. HSI has many applications in agriculture, urban planning, geology, and environmental studies [1-3]. An HSI contains a wealth of spatial and spectral information, requiring advanced pattern recognition and image processing techniques to process. With the advancement of electronics science and the development of high-resolution hyperspectral sensors, spatial features are being used as additional information to improve the accuracy of HSI classification [4]. It is challenging to classify HSI due to the curse of dimensionality, the small training sample size, the significant within-class spectral variations, and low between-class spectral variations[5].

To date, various methods have been proposed in the literature to address these issues. Different dimensionality reduction methods, such as principal components analysis (PCA), minimum noise fraction (MNF) transform, linear discriminant analysis (LDA), clustering-based, and optimization-based methods, are proposed in the literature to handle the high dimensionality of HSIs [6-9]. The second problem is addressed using advanced classification methods, such as support vector machine (SVM), extreme learning machine (ELM), and random multigraphs (RMG), which can produce accurate classification results in the situation of small training samples [10-13]. A variety of sample expansion and augmentation techniques have been used to increase the number of training samples to improve classification accuracy [14-16]. The third challenge, spectral variability, is generally addressed by incorporating spatial features in the classification process [17-19]. According to the literature, Gray-level co-occurrence matrix (GLCM), extended morphological profiles, attribute profiles, Gabor filters, moment invariants, local binary patterns, wavelets, fractal features, guided filters, and deep-learning-based features are some of the most important spatial features generation methods used in the classification of HSIs [11, 13, 19, 20]. Stacking spatial and spectral features is a

popular feature combination method for HSI classification. Although this method is efficient and straightforward, it neglects local relationships between features, which can be useful in HSI classification.

Tuzel et al. introduced covariance matrix descriptors (CMD) for object and texture detection in the computer vision field [21]. The covariance matrix is a powerful feature descriptor for evaluating the linear relationships between features. After that, CMD is employed in several computer vision and image processing studies, such as face recognition and action recognition [22, 23]. Recently, Fang et al. used local covariance matrix descriptors (LCMD) of pixels and log-Euclidean kernel SVM to classify HSIs [24]. Accordingly, local covariance matrix descriptors are used in several studies to classify HSI. Zhao et al. combined the density peak clustering and covariance matrix representation for HSI classification [25]. He et al. propose a deep-learning-based method based on multiscale covariance representations for HSI classification [26]. A new study combines covariance matrix representation with a deep random patch network to classify HSI [27]. A new classification method for HSI is also proposed based on multiscale adaptive weighted filtering and covariance matrix representation [28]. Despite being a simple and efficient local descriptor, the covariance matrix representation has three major limitations. These include the singularity of LCMD in small window sizes, a fixed shape representation, and the inability to evaluate nonlinear relationships between features [29].

A kernel matrix descriptor (KMD) is proposed in computer vision to address these issues [29, 30]. As an important note, a kernel matrix can evaluate nonlinear relationships and higher-order statistics of features. A traditional covariance matrix is a particular form of the kernel matrix when using a linear kernel [29]. The KMD has been studied in various areas of image processing and computer vision, but its performance for HSI classification has not yet been evaluated. As a result, this research aims to develop the concept of local kernel matrix descriptors (LKMD) for HSI classification. A comparison is also made between the performance of LKMD with two different kernel functions and LCMR. LKMD is expected to improve the classification accuracy of HSI due to its ability to evaluate nonlinear relationships between features.

The following sections of the article are as follows: Concepts of LCMD and LKMD and log-Euclidean SVM are presented in the next section. Section 3 introduces the HSI datasets used in this work. Experimental results are provided in section 4, and finally, the last section concludes the study.

2. Methodology

The proposed method of this study is depicted in Fig. 1. In the first stage, the MNF dimensionality reduction method is applied to the original HSI to extract the more informative features and eliminate the redundant spectral features. In the second stage, as the spatial-spectral feature generation methods, both types of local matrix features, LCMD and LKMD, are generated. These matrix-based features are fed to supervised log-Euclidean kernel SVM in the third stage to classify HSI. Finally, classification accuracy based on test samples is used to compare the performance of local descriptors. The following subsections provide more information on the LCMD, LKMD, and log-Euclidean kernel SVM.

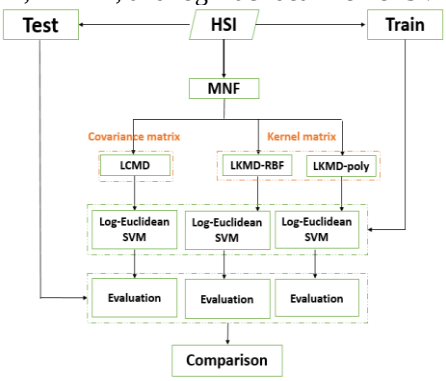

Fig. 1. Flowchart of the proposed method

A) The LCMD and LKMD

The covariance matrix as the linear kernel can model the linear relationship between the hyperspectral bands. Assume a sliding window with size (L) around each pixel (total pixels in the widow is $R=L\times L$) of HSI with the N number of the spectral features. The LCMD with the size $N\times N$ for each pixel is defined as [24]:

$$LCMD = \frac{1}{R-1}\sum_{i=1}^{R}(x_i-\mu).(x_i-\mu)^T \quad (1)$$

In which x_i is the feature vector of an i^{th} pixel in window L, and μ is the mean vector.

A kernel matrix descriptor has recently been proposed in computer vision to address the limitations of the covariance descriptor. Different kernels, such as RBF and Polynomial kernels, have different abilities to evaluate the nonlinear relationship of the features [29]. This paper aims to compare them with LCMD. Similar to LCMD, assume a sliding window with size ($L\times L$) around each pixel. In this window, each band of HSI can be expressed as the y_i ($i=1$ *to* N) vector with the dimension equal to $R=L\times L$. Each element of the LKMD matrix (with the size of $N\times N$) with RBF and polynomial kernel are calculated with [29]:

$$k_{RBF}(y_i,y_j) = \exp\left(-\beta||y_i-y_j||^2\right) \quad (2)$$

$$k_{Poly}(y_i, y_j) = (||y_i - y_j||^2 + \beta^2)^{-1/2} \quad (3)$$

Where β is the scaling parameter of kernels that is set to 0.1 based on trial and error. A regularization technique can be used to make both LCMD and LKMD strictly positive defined.

B) Log-Euclidean kernel SVM

The symmetric positive definite (SPD) matrices such as LCMD and LKMD lie on a manifold. The SPD matrix cannot be classified using SVM with standard kernels. The SVM with log-Euclidean kernel function (k_{logm}) is the best choice for classifying SPD matrices, which is defined for two different SPD matrices, C_1 and C_2, as follows [24]:

$$k_{logm}(C_1, C_2) = trace[logm(C_1).logm(C_2)] \quad (4)$$

logm is the logarithm of the matrix.

3. Hyperspectral datasets

***Indian Pines*:** The Indian Pines dataset is a benchmark HSI collected by the AVIRIS sensor from an agricultural and semi-urban area in Indiana, the USA, with a spatial resolution of 20m. This image contains 145×145 pixels in 224 spectral bands. After removing the 24 noisy bands in the pre-processing stage, the remaining 200 bands are used in the experiment. Based on the ground truth map (GTM) of this image, this scene contains the 16 agricultural classes. The unbalanced distribution of the classes makes the classification of this image difficult. Fig. 2-a depicts a color composite of the Indian Pines dataset.

***Pavia University*:** The Pavia University dataset from an urban area is the second benchmark HSI. This image was captured by a ROSIS-3 hyperspectral camera from the University of Pavia, with a spatial resolution of 1.3 m. This image contains 610×340 pixels with 115 spectral bands. After removing the 12 noisy bands, the experiments use the remaining 103 bands. Based on the GTM of the image, this scene contains the nine urban classes. Fig. 2-b depicts a color composite of this HSI.

4. Experimental results

In this study, ten samples from each class are randomly selected based on ground truth maps (GTMs) of each HSI as training samples, with the rest serving as tests for assessing the classification results. The experiments employ four classification metrics for accuracy evaluation: overall accuracy (OA), average accuracy (AA), kappa coefficient (kappa), and class accuracy [31].

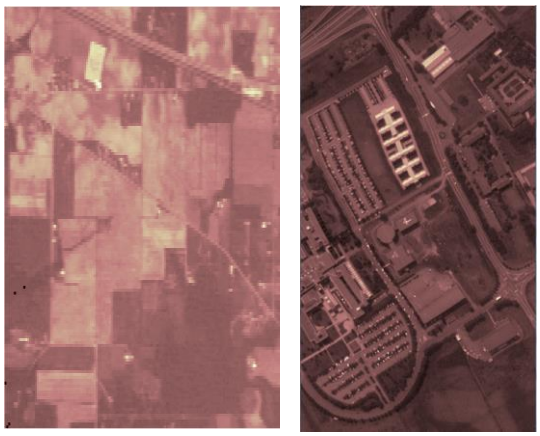

a b

Fig. 2. HSI Datasets. a) Indian Pines. b) Pavia University

For LCMD and LKMD, two parameters should be tuned: window size (*w*) and the number of MNF components (#MNF). We analyzed these two parameters in our first experiment, and the results are shown in Fig. 3. Based on Fig. 3, the optimum values of #MNF and *w* for the LCMD method are 25 and 23 in the Indian Pines dataset, respectively, and 25 and 15 for the Pavia University dataset. The optimal values of #MNF and *w* for LKMD with RBF kernel are 25 and 7 for Indian pines and 15 and 7 for Pavia University, respectively. The optimum values of #MNF and *w* for the LKMD-Poly for both data are 25 and 7. Although we did not see a single optimum parameter combination for each method in each dataset, as the rule of the thumb for LKMD methods, appropriate results are achieved when more MNF components are selected, and the *w* is considered between 7 and 11.

The second experiment compares the classification results of spectral features, LCMD, and LKMD. SVM with an RBF kernel is used for spectral-based classification of HSI, and SVM with a log-Euclidean kernel is used to classify LCMD and LKMD. For both datasets, the classification results of each method are shown in Tables 1 and 2.

According to Tables 1 and 2, both LCMD and LKMD can improve the accuracy of HSI classification. This is due to LCMD and LKMD's ability to evaluate the local relationships between the features. Generally, LKMD achieves higher accuracy than LCMD due to considering nonlinear local relationships between features. Based on the results, LKMD-RBF and LKMD-Poly appear to have a comparable performance. LKMD-Poly may perform better in low-resolution HSI from agricultural regions, such as Indian Pines. In contrast, LKMD-RBF may perform better in high-resolution HSI from urban areas, such as Pavia University.

Fig. 4 and Fig. 5 show the final classified images for each method. Based on these figures, it is

straightforward that both LCMD and LKMD can generate smoother classified images than the original spectral-based HSI classification. It demonstrated the effectiveness of using spatial information to increase the classification accuracy of HSI once more.

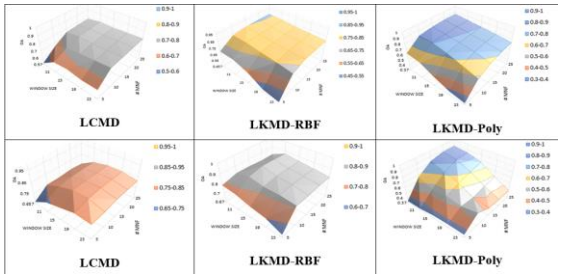

Fig. 3. Parameters settings) first row Indian Pines, second row Pavia University

Table.1.
Classification results of Indian Pines

Class	*Methods*			
	Spectral	*LCMD*	*LKMD*	
			RBF	Poly
1	72.22	100	100	100
2	35.61	62.69	83.14	84.34
3	37.56	79.14	94.39	93.41
4	65.19	80.61	88.10	84.14
5	58.59	83.93	93.65	94.08
6	86.25	83.61	99.30	98.47
7	94.44	100	100	100
8	75.85	98.5	100	100
9	100	100	100	100
10	44.59	76.19	82.32	82.01
11	45.76	70.59	67.23	68.79
12	55.57	76.84	86.45	86.96
13	94.87	97.43	98.46	97.94
14	64.30	97.13	97.92	97.29
15	49.73	98.93	90.42	92.28
16	95.18	93.97	100	100
OA	53.49	79.40	85.51	85.83
AA	67.23	87.48	92.59	92.48
Kappa	0.473	0.769	0.835	0.8405

Table.2.
Classification results of Pavia University

Class	***Methods***			
	Spectral	***LCMD***	***LKMD***	
			RBF	***Poly***
1	75.27	69.85	73.61	79.68
2	75.65	88.16	94.75	95.05
3	58.30	80.46	70.84	76.59
4	80.12	80.09	95.05	91.74
5	99.62	99.85	100	100
6	75.21	95.13	95.33	88.08
7	76.89	84.62	99.09	88.71
8	65.63	78.73	73.26	66.61
9	99.46	77.04	93.59	95.94
OA	75.46	84.28	88.82	88.24
AA	78.46	83.22	88.4	86.94
Kappa	0.683	0.796	0.8536	0.845

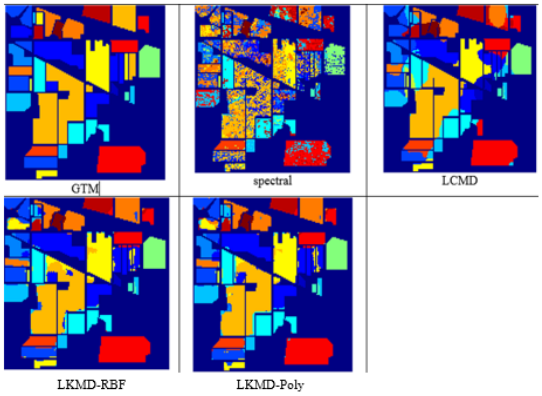

Fig. 4. GTM and classified images of the Indian Pines scene

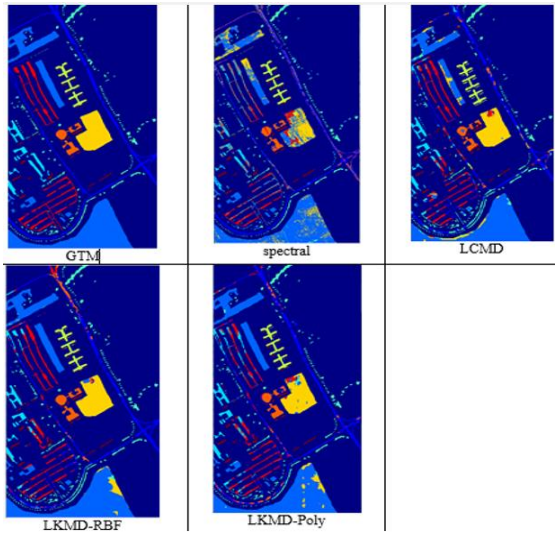

Fig. 5. GTM and classified images of the Pavia University scene

5. Conclusions

According to recent research, the local covariance matrix is a new spatial-spectral feature descriptor that considers the local linear relationship of features. However, because of the complex relationship between the features in the HSI, it seems that local kernel features that can evaluate the local nonlinear relationships and higher-order statistics can better represent the HSI. In this study, two types of local kernel matrix descriptors, RBF and polynomial kernels are compared with the covariance matrix. The final results on the two HSIs demonstrated that the local kernel matrix descriptors outperformed the local covariance matrix descriptors in HSI classification. In future research, we will create a local combined multi-kernel matrix descriptor for HSI classification based on the fusion of RBF and polynomial kernels.

References

[1] Van der Meer, F.D., Van der Werff, H.M., Van Ruitenbeek, F.J., Hecker, C.A., Bakker, W.H., Noomen, M.F., Van Der Meijde, M., Carranza, E.J.M., De Smeth, J.B. and Woldai, T. "Multi-and hyperspectral geologic remote sensing: A review," International Journal of Applied Earth Observation and Geoinformation, 2012. 14(1): p. 112-128.

[2] Adão, T., Hruška, J., Pádua, L., Bessa, J., Peres, E., Morais, R. and Sousa, J.J. "Hyperspectral imaging: A review on UAV-based sensors, data processing and applications for agriculture and forestry," Remote sensing, 2017. 9(11): p. 1110.

[3] Lu, B., Dao, P.D., Liu, J., He, Y. and Shang, J. "Recent advances of hyperspectral imaging technology and applications in agriculture," Remote Sensing, 2020. 12(16): p. 2659.

[4] Zhao, W. and S. Du. "Spectral–spatial feature extraction for hyperspectral image classification: A dimension reduction and deep learning approach," IEEE Transactions on Geoscience and Remote Sensing, 2016. 54(8): p. 4544-4554.

[5] Asghari Beirami, B. and M. Mokhtarzade. "Spatial-Spectral Classification of Hyperspectral Images Based on Extended Morphological Profiles and Guided Filter," Computer and Knowledge Engineering, 2020. 2(2): p. 2-8.

[6] Beirami, B.A. and M. Mokhtarzade. "Band grouping superpca for feature extraction and extended morphological profile production from hyperspectral images," IEEE Geoscience and Remote Sensing Letters, 2020. 17(11): p. 1953-1957.

[7] Beirami, B.A. and M. Mokhtarzade. "An Automatic Method for Unsupervised Feature Selection of Hyperspectral Images Based on Fuzzy Clustering of Bands," Traitement du Signal, 2020. 37(2).

[8] Beirami, B.A. and M. Mokhtarzade. "Superpixel-Based Minimum Noise Fraction Feature Extraction for Classification of Hyperspectral Images," Traitement du Signal, 2020. 37(5).

[9] Moghaddam, S.H.A., M. Mokhtarzade, and B.A. Beirami. "A feature extraction method based on spectral segmentation and integration of hyperspectral images," International Journal of Applied Earth Observation and Geoinformation, 2020. 89: p. 102097.

[10] Miao, Y., Chen, M., Yuan, Y., Chanussot, J. and Wang, Q. "Hyperspectral Imagery Classification via Random Multigraphs Ensemble Learning," IEEE Journal of Selected Topics in Applied Earth Observations and Remote Sensing, 2021. 15: p. 641-653.

[11] Gao, F., Wang, Q., Dong, J. and Xu, Q. "Spectral and spatial classification of hyperspectral images based on random multi-graphs," Remote Sensing, 2018. 10(8): p. 1271.

[12] Ergul, U. and G. Bilgin. "MCK-ELM: multiple composite kernel extreme learning machine for hyperspectral images," Neural Computing and Applications, 2020. 32(11): p. 6809-6819.

[13] Guo, Y., Yin, X., Zhao, X., Yang, D. and Bai, Y. "Hyperspectral image classification with SVM and guided filter," EURASIP Journal on Wireless Communications and Networking, 2019. 2019(1): p. 1-9.

[14] Zhao, W., Chen, X., Chen, J. and Qu, Y. "Sample generation with self-attention generative adversarial adaptation network (SaGAAN) for hyperspectral image classification," Remote Sensing, 2020. 12(5): p. 843.

[15] Li, W., Chen, C., Zhang, M., Li, H. and Du, Q. "Data augmentation for hyperspectral image classification with deep CNN," IEEE Geoscience and Remote Sensing Letters, 2018. 16(4): p. 593-597.

[16] Haut, J.M., Paoletti, M.E., Plaza, J., Plaza, A. and Li, J. "Hyperspectral image classification using random occlusion data augmentation," IEEE Geoscience and Remote Sensing Letters, 2019. 16(11): p. 1751-1755.

[17] Seifi Majdar, R. and H. Ghassemian. "A probabilistic framework for weighted combination of multiple-feature classifications of hyperspectral images," Earth Science Informatics, 2020. 13(1): p. 55-69.

[18] Beirami, B.A. and M. Mokhtarzade. "Classification of Hyperspectral Images based on Intrinsic Image Decomposition and Deep Convolutional Neural Network," in 2020 6th Iranian Conference on Signal Processing and Intelligent Systems (ICSPIS). 2020. IEEE.

[19] Beirami, B.A. and M. Mokhtarzade. "Spatial-spectral classification of hyperspectral images based on multiple fractal-based features," Geocarto International, 2022. 37(1): p. 231-245.

[20] Beirami, B.A. and M. Mokhtarzade. "Spatial-Spectral Random Patches Network for Classification of Hyperspectral Images," Traitement du Signal, 2019. 36(5).

[21] Tuzel, O., F. Porikli, and P. Meer. "Region covariance: A fast descriptor for detection and classification," in European conference on computer vision. 2006. Springer.

[22] Hariri, W., Tabia, H., Farah, N., Benouareth, A. and Declercq, D. "3D face recognition using covariance based descriptors," Pattern Recognition Letters, 2016. 78: p. 1-7.

[23] Hussein, M.E., Torki, M., Gowayyed, M.A. and El-Saban, M. "Human action recognition using a temporal hierarchy of covariance descriptors on 3d joint locations," in Twenty-third international joint conference on artificial intelligence. 2013.

[24] Fang, L., He, N., Li, S., Plaza, A.J. and Plaza, J. "A new spatial–spectral feature extraction method for hyperspectral images using local covariance matrix representation," IEEE Transactions on Geoscience and Remote Sensing, 2018. 56(6): p. 3534-3546.

[25] Zhao, G., Li, N., Tu, B., Zhang, G. and He, W. "Density peak covariance matrix for feature extraction of hyperspectral image," IEEE Geoscience and Remote Sensing Letters, 2019. 17(3): p. 534-538.

[26] He, N., Paoletti, M.E., Haut, J.M., Fang, L., Li, S., Plaza, A. and Plaza, J. "Feature extraction with multiscale covariance maps for hyperspectral image classification," IEEE Transactions on Geoscience and Remote Sensing, 2018. 57(2): p. 755-769.

[27] Sun, Y., Z. Fu, and L. Fan, "A novel hyperspectral image classification pattern using random patches convolution and local covariance," Remote Sensing, 2019. 11(16): p. 1954.

[28] Zhang, X., Wei, Y., Yao, H. and Zhou, Y. "Improved local covariance matrix representation for hyperspectral image classification," in IGARSS 2020-2020 IEEE International Geoscience and Remote Sensing Symposium. 2020. IEEE.

[29] Wang, L., Zhang, J., Zhou, L., Tang, C. and Li, W. "Beyond covariance: Feature representation with nonlinear kernel matrices," in Proceedings of the IEEE International Conference on Computer Vision. 2015.

[30] Zhang, J., Wang, L., Zhou, L. and Li, W. "Beyond covariance: Sice and kernel based visual feature representation," International Journal of Computer Vision, 2021. 129(2): p. 300-320.

[31] Beirami, B.A. and M. Mokhtarzade. "SVM classification of hyperspectral images using the combination of spectral bands and Moran's I features," in 2017 10th Iranian Conference on Machine Vision and Image Processing (MVIP). 2017. IEEE.